Micro- and macrosegregation of a peritectic Au–Fe alloy during Bridgman solidification

Denis Favez[1], Michel Rappaz[1]

[1]Computational Materials Laboratory
Ecole Polytechnique Fédérale de Lausanne
CH-1015 Lausanne, Switzerland

Keywords: Au–Fe system, peritectic, microsegregation, macrosegregation

Abstract

In jewelry manufacturing, joining dissimilar materials is usually achieved by soldering or brazing, but these techniques have several disadvantages as compared for example with laser welding. In this last case, however, it is necessary to have a thorough understanding of microstructure formation during solidification. Microstructure analysis of quenched Bridgman solidified specimens provides access to a wide range of information on solidification phenomena, as for example micro- and macrosegregation. The present study focuses on a peritectic Au–Fe alloy solidified at low speed in a high thermal gradient. Micro- and macrosegregation are investigated through microstructure analysis and modeling. On one hand, microsegregation along secondary dendrite arms is measured with a microprobe. These results are compared with simple 1D front-tracking numerical simulations of microsegregation, coupled with the available phase diagram and accounting for the peritectic reaction. On the other hand, strong macrosegregation is observed during solidification of Au–Fe alloy, due to the high density difference between iron and gold. An analysis based on solidification shrinkage and the model of Flemings and Nereo is presented.

Introduction

During laser welding of dissimilar materials such as gold and steel for jewelry applications, base metals are more or less mixed in the weld pool, depending on convection. This may lead to the formation of various phases upon solidification. Moreover, the local composition of the weld pool being strongly dependent on laser beam position, quite complex solidification microstructures can form. A more fondamental metallurgical study of the solidification of a mixture of these alloys could then provide useful information. For example, interrupted Bridgman solidification of well-defined composition alloys gives access to the complete chronology of microstructure formation for fixed solidification velocity V and thermal gradient G.

In the present study, a hypoperitectic Au–Fe alloy with 22 at.% Au has been solidified at low speed in a high thermal gradient. According to the phase diagram (Fig. 1), solidification starts with the formation of austenite (γ-Fe) at 1360°C, which grows up to 1173°C where the peritectic reaction (γ-Fe) + $\ell \rightarrow$ (Au) occurs. It should be noted here that both (γ-Fe) and (Au) phases are actually the same *fcc* phase that undergoes a miscibility gap.

Within this solidification interval, a partition coefficient k around 0.2 induces a significant solute rejection in the liquid, which may give rise to microsegregation. However, an important solid state diffusion at these high temperatures tends to homogenize the composition. Furthermore the strong density difference between gold and iron induces macrosegregation.

In order to quantify the extent of micro- and macrosegregation during Bridgman solidification, microprobe and SEM image analysis are compared with modeling.

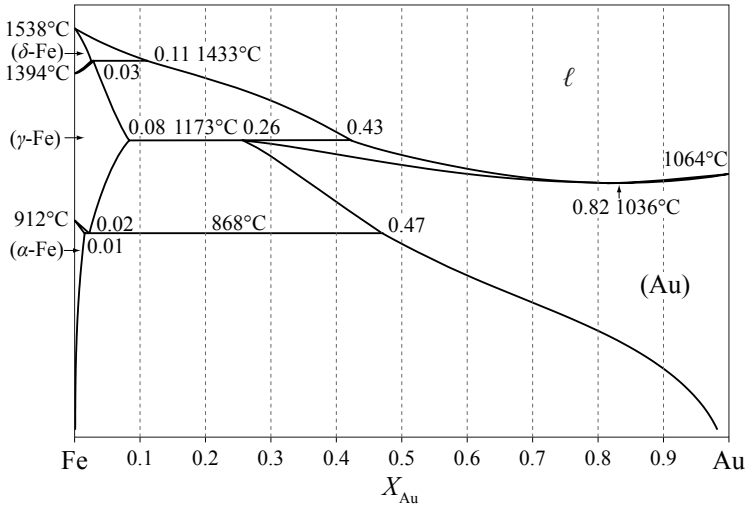

Figure 1: Au–Fe phase diagram (redrawn from [1])

Materials and methods

Bridgman solidification

Directional solidification experiments were undertaken on Au–Fe alloy with 22 at.% gold, an hypoperitectic composition. As base metals, iron powder and gold pellets were used, both of 99.99 wt% purity.

The samples were solidified in a high thermal gradient vertical Bridgman furnace [2], which consisted of a heater, a hollow molybdenum susceptor placed in a protective atmosphere and heated by an induction coil, and a cooler, a water-cooled liquid metal bath. The Au–Fe alloy was placed in a cylindrical alumina crucible of inner/outer diameter of 4/6 mm. The complete procedure is detailed elsewhere [3].

Figure 2 (left) shows the quenched microstructure of a sample solidified at 1.7 µm/s in a thermal gradient of 3×10^4 K/m. With these solidification parameters, a dendritic microstructure forms with a typical secondary arms spacing between 20 µm at the dendritic front and 60 µm close to the peritectic temperature T_p [3]. As will be detailed hereafter, the convex shape of the dendritic front can be related to macrosegregation. The solidification ends with the formation of the peritectic phase (Au) around 1165°C, with a composition around 26 at.%.

Sample preparation and analysis

After quenching, the cylindrical samples were sectioned along their longitudinal axis, mounted in a classical conducting resin and polished down to 1 µm. SEM analysis has been conducted using back-scattered electrons (BSE), which give a direct information on the local composition due to the high difference in atomic number between gold (79) and iron (26). Thus, the grey levels revealed by SEM BSE images can be taken as composition maps that can be treated subsequently by an image analysis program.

Microsegregation analysis In order to measure precisely the microsegregation profile in secondary dendrite arms along the temperature gradient, WDS microprobe analysis was performed using a JEOL 8200 microprobe. Composition profiles of around 80 µm length were

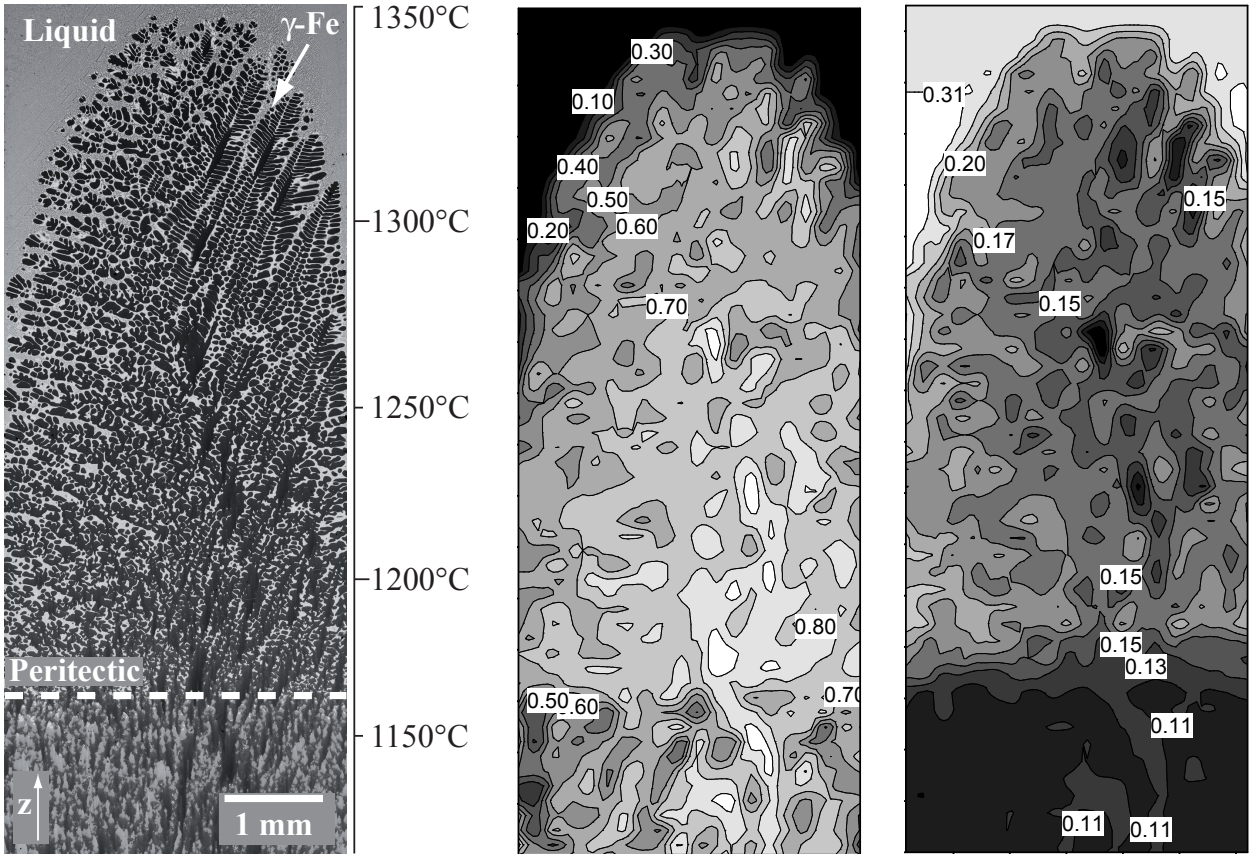

Figure 2: Left: SEM BSE image of a longitudinal section of Au–Fe (22 at.% Au) solidified at $V = 1.7$ µm/s in a thermal gradient $G = 300$ K/cm. Center: Corresponding volume fraction of primary (γ-Fe). Right: Corresponding average atomic fraction $\langle X \rangle_M$

taken in the center of the specimen for four temperatures ranging between the dendritic front and the peritectic reaction. At each temperature, four to five profiles have been recorded. As will be shown, the liquid and primary (γ-Fe) phase compositions are fairly uniform at the microstructure scale (i.e., lever rule).

Macrosegregation analysis Macrosegregation has been characterized by the average average mass composition $\langle c \rangle_M = c_s f_s + c_l f_l$. As metallography gives a direct access to the volume fractions g instead of the mass fractions f, it is more convenient to express $\langle c \rangle_M$ of a small element of homogeneous composition as

$$\langle c \rangle_M = \frac{\rho_s c_s g_s + \rho_l c_l g_l}{\rho_s g_s + \rho_l g_l} \tag{1}$$

Local volume fractions have been measured by image analysis of the complete solidification sequence SEM BSE image. The volume fraction of primary (γ-Fe) phase is shown in the central map of Fig. 2. An open-source image analysis software [4] was used to divide the image into 200 µm x 200 µm squares. As grey levels are related to composition in SEM BSE images, the volume fractions could be directly deduced from the relative amount of pixels that are within specified ranges. Local compositions c (or atomic fractions X) of various phases have been extrapolated at any z-position from the microprobe measurements performed at four heights (see Fig. 2 left), using a third-order polynomial interpolation. Finally, local liquid and solid densities have been calculated using the mixing rule $\rho_l(z) = X_{Au}(z)\rho_{l,Au} + (1 - X_{Au}(z))\rho_{l,Fe}$, $\rho_{l,Au}$ and $\rho_{l,Fe}$ being the density of pure liquid elements averaged over the solidification range ($\partial\rho/\partial c \gg \partial\rho/\partial T$) [5]. Considering the small variation in the solid composition of (γ-Fe) and (Au) near the peritectic temperature T_p, these two solid phases were considered to have a fixed density (but $\rho_{(\gamma-\mathrm{Fe})} \neq \rho_{(\mathrm{Au})}$).

In order to be consistent with microsegregation results, calculated average mass compositions $\langle c \rangle_M$ were subsequently converted into atomic fractions $\langle X \rangle_M$.

Microsegregation

Model

The microsegregation model considers a small volume element of one dendrite secondary arm, which is assimilated to a 1D domain of fixed size initially composed of two phases (solid and liquid) separated by a sharp interface (see Fig. 3, left). The x-axis of this element corresponds then to the vector connecting the secondary arm center ($x = 0$) to the mid-point between two secondary arms in the liquid ($x = \lambda_2/2 = L$), $x^*(t)$ being the position of the interface.

This element is cooled at a constant rate $\dot{T} = VG$ related to the crucible velocity in the Bridgman furnace V and the thermal gradient G. With cooling, compositions at the interface evolves as dictated by the phase diagram. The displacement of the interface is then assumed to be governed by solute diffusion only. The velocity of the interface $v^*(t)$, which determines x^* by integration, is calculated from the solute balance:

$$v^*(c_l^* - c_s^*) = \tilde{D}_s(T) \left(\frac{\partial c_s}{\partial x} \right)_{x^*} - \tilde{D}_l(T) \left(\frac{\partial c_l}{\partial x} \right)_{x^*} \tag{2}$$

where $\tilde{D}_s(T)$ is the inderdiffusion coefficient in the solid, $\tilde{D}_l(T)$ is the interdiffusion coefficient in the liquid, and $c_\nu(x,t)$ the concentration profile in each phase ($\nu = s, l$).

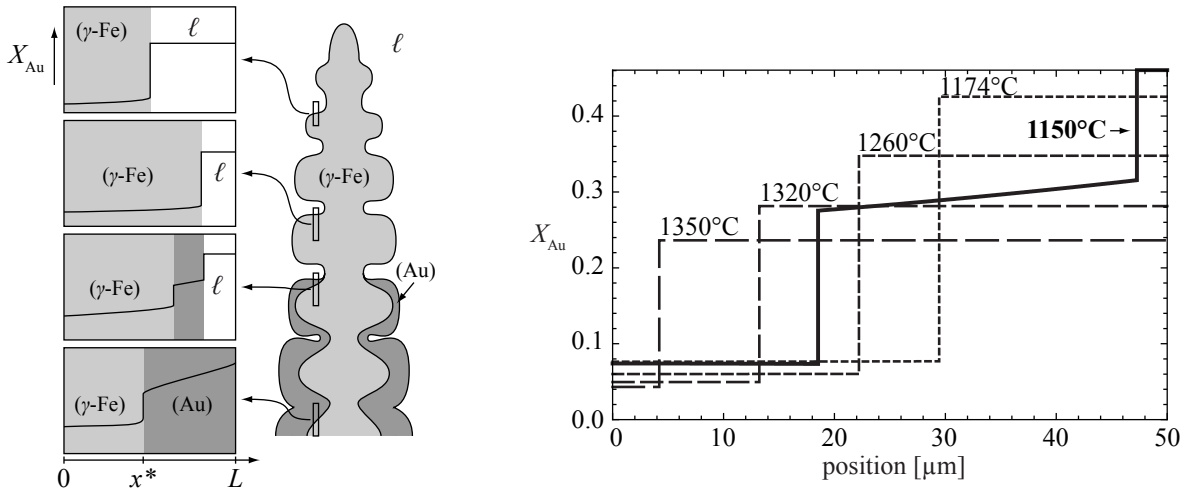

Figure 3: Left: Schematic diagram of the microsegregation model. The problem is reduced to a 1D domain cooled down at a fixed rate $\dot{T}$. Right: Results of numerical simulation: composition profile at various temperatures during primary solidification (dashed lines) and peritectic reaction (thick line). Microsegregation occurs according to lever rule for primary solidification and according to Scheil–Gulliver model once the peritectic phase (Au) forms.

The diffusion in each phase is calculated using Fick's second law, with the interdiffusion coefficient in the solid phase given by:

$$\tilde{D}_s(x,T) = X_{\mathrm{Au}}(x,T)D_{(\gamma-Fe)}(T) + (1 - X_{\mathrm{Au}}(x,T))D_{\mathrm{Au}}(T) \tag{3}$$

where $D_{(\gamma-Fe)}(T)$ and $D_{\mathrm{Au}}(T)$ are self-diffusion coefficients of pure *fcc* iron and gold, taken from [5], and $X_{\mathrm{Au}}(T)$ is the gold atomic fraction of the corresponding node. This approach is known to be not satisfactory for the Au–Fe system [6] but has nevertheless been used as an approximation in the calculations, as no other method seems available. The interdiffusion coefficient in the liquid phase has been assumed to be equal to the self-diffusion coefficient of pure gold [7]. It has no real influence as near complete mixing is reached in this phase. Constant density and homogeneous temperature within the element are also taken as hypotheses and no flux is considered at $x = 0$ and $x = L$.

The front tracking method used here consists in a finite difference method and an adaptative mesh with a fixed number of nodes in each phase. At each time step, the interface velocity is calculated with the help of equation (2) and the mesh is stretched accordingly. Then, an implicit scheme is employed to solve the diffusion equations in each phase.

Initial conditions are one liquid domain of homogeneous composition $c_l = 0.5$ ($X_l = 0.22$), with a thin (nucleated) solid phase, whose composition is dictated by the phase diagram. The interface is arbitrarily placed at $x^* = 10^{-5}L$. Then, at each time step dt, the temperature is decreased by $\dot{T}dt$.

At the peritectic temperature T_p, a new domain with the peritectic composition of (Au) is inserted as a thin layer between the primary (γ-Fe) and the liquid. Then, the same calculation as described before is applied to both interfaces ((γ-Fe)–(Au) and (Au)–liquid). As both primary (γ-Fe) and peritectic phase (Au) share the same crystal structure, the interdiffusion coefficient for the (Au) phase has been taken as described by equation (3).

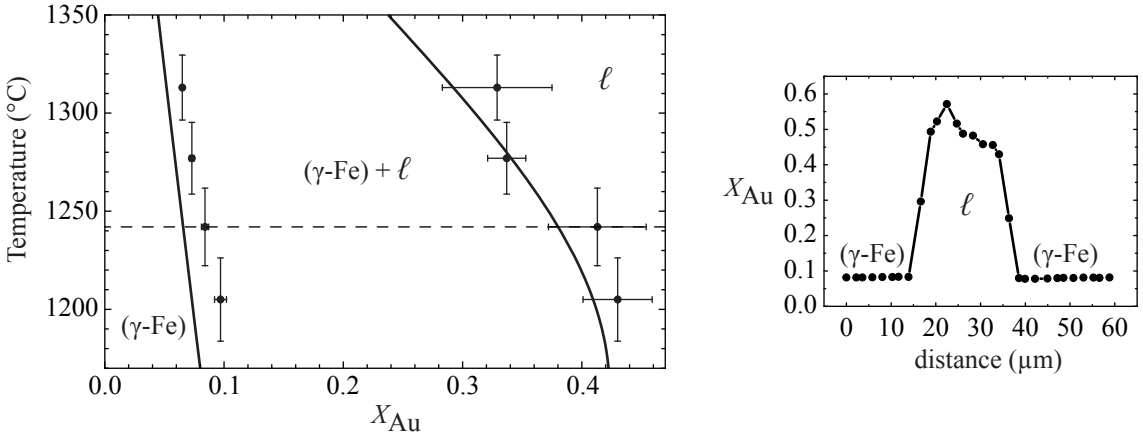

Figure 4: Left: Microprobe measurements in the solid (γ-Fe) and liquid phase measured at four heights in the speciment shown on Fig. 2. Temperature error bars are due to position uncertainty of microprobe measurements with respect to the furnace thermal gradient. Composition error bars for the liquid phase are related to the strong microsegregation of this phase during quenching. These data are superimposed with the phase diagram from [1]. Right: Example of one microprobe measurement at the temperature indicated by the dashed line.

Numerical solution

The results of a simulation with a domain size of 50 µm is presented in Fig. 3 (right). It can be seen that no microsegregation is observed during the primary solidification. Composition is homogeneous in both solid and liquid phases, and thus follows lever rule. On the contrary, formation of the peritectic phase (Au) shows a strong microsegregation and composition gradient in the (Au) phase.

Experimental results

Microprobe measurements show a good correlation with the microsegregation model: microsegregation obeys lever rule between the liquidus and peritectic temperature T_p, whereas the peritectic phase (Au) shows a fairly strong microsegregation. However, microprobe measurements of the (γ-Fe) phase composition are slightly shifted with respect to the phase diagram(see Fig. 4). Even if the position of the microprobe measurements with respect to the furnace thermal gradient is not precisely known ($\pm$0.8 mm, see error bars on the temperature scale), the data are still slightly off with respect to the liquidus and solidus of [1]. The liquid phase composition is less precisely measured, as can be seen on Fig. 4 (right) due to the quench. The plotted values are then averaged over the liquid phase, the error bars corresponding to the standard deviation.

Furthermore, as indicated by the microsegregation model (Fig. 3) and experimental measurements (Fig. 2), the peritectic reaction takes place over a short temperature interval (25 K and 15 K, respectively).

This difference in microsegregation profile between primary and peritectic solidification can be related to the phase diagram (Fig. 1) and the Fourier number Fo:

$$\mathrm{Fo} = \frac{4\tilde{D}_s \Delta T}{(\lambda_2)^2 \left|\dot{T}\right|} \tag{4}$$

where $\tilde{D}_s$ is the diffusion coefficient in the solid phase and ΔT the solidification interval. A high Fourier number tends to give a solidification according to lever rule, whereas a low Fo makes it closer to the Scheil-Gulliver model [8]. As $(\lambda_2)^2|\dot{T}|$ is kept constant in both primary solidification and peritectic reaction, the difference between those must be found in the $\tilde{D}_s\Delta T$ term. The interdiffusion coefficient of the (γ-Fe) phase ranges between 2.6×10^{-11} m^2/s and 4.1×10^{-12} m^2/s, while it is of 3.4×10^{-12} m^2/s for the (Au) phase. Furthermore, the solidification interval also differs: 200 K for the (γ-Fe) phase to 25 K or 15 K for the (Au) phase. Thus, taking $\lambda_2/2 = 50$ µm and $|\dot{T}| = 0.034$ K/s, the Fourier number for the solidification of (γ-Fe) phase (calculated with a mean interdiffusion coefficient of 1.1×10^{-11} m^2/s) is $\mathrm{Fo}_{(\gamma-\mathrm{Fe})} = 25$ indicating lever rule, while the Fourier number associated with the peritectic reaction is $\mathrm{Fo}_{(\mathrm{Au})} = 0.6$, closer to a Scheil–Gulliver approximation. This dimensionless number analysis explains then the microsegregation profiles.

Macrosegregation

Model

Macrosegregation induced by solidification shrinkage has been described by Flemings and Nereo [9]. The authors assumed that: (i) the density of the solid phase is constant; (ii) the solid is fixed; (iii) microsegregation occurs as dictated by the lever rule; and (iv) solidification as well as interdendritic flow are one dimensional, e.g., along the z-direction. They showed that, everywhere in the mushy zone, the velocity of the liquid is given by:

$$v_{ly} = -\beta(c_l)v_T \tag{5}$$

where $\beta(c_l) = \rho_s/\rho_l(c_l) - 1$ is the shrinkage factor and v_T the velocity of the isotherms.

Furthermore, these authors calculated the average mass composition within the mushy zone under steady state conditions and lever-rule approximation to be equal to:

$$\frac{\langle c\rangle_M}{c_0} = \frac{c_l\rho_l g_l + c_s\rho_s g_s}{(\rho_s g_s + \rho_l g_l)\left(g_l\left(c_l - c_s\right) + c_s\right)} \tag{6}$$

During primary solidification of Au–Fe with 22 at.% Fe, $\beta(c_l)$ is strongly negative, as shown on Fig. 5, due to the rejection of heavy Au solute element. The solid phase being less dense than the liquid phase, solidification should induce liquid expulsion from the mushy zone. Therefore, under steady state condition, positive macrosegregation in the mushy zone is expected as well as $\langle c\rangle_M = c_0$ (no macrosegregatoin) after complete solidification. In other words, according to equation (6), $\langle c\rangle_M$ is equal to c_0 for $g_l = 0$ and $g_l = 1$, and $\langle c\rangle_M > c_0$ in between.

Experimental results

However, experimental measurements of $\langle X\rangle_M$ rather indicate negative macrosegregation: Fig. 2 (right) shows $\langle X\rangle_M$ in the mushy zone being rather around 15 at.%–17 at.% than 22 at.% about T_p. Actually, the 1D hypothesis is not verified in the present case, as shown by the strong curvature of the dendritic front on the SEM image (see Fig. 2 (left)).

The negative sign of $\beta(c_l)$ indicates that solute-rich liquid (i.e denser than liquid of nominal composition) is rejected from the mushy zone. As the thermal gradient in this Bridgman experiment goes upward, this rejected liquid will accumulate at the dendritic front, due to gravity. If the front were planar, this accumulation would induce no convection

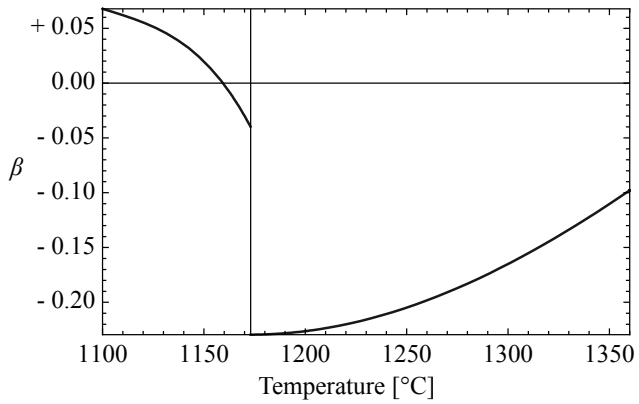

Figure 5: Shrinkage factor $\beta(c_l) = \rho_s/\rho_l(c_l) - 1$ as a function of temperature for the Au–Fe system. Above T_p, β is strongly negative, indicating that interdendritic liquid is expelled from the mushy zone. Below T_p, β for direct solidification of the peritectic phase (Au) is close to zero, i.e. almost no volume change occurs during peritectic direct solidification.

the situation would remain 1D and the final composition should be equal to c_0 after complete solidification.

However, as it can be seen on Fig. 2 (left), the dendritic front has a strongly convex shape. This is due to the presence of a small radial thermal gradient in the Bridgman furnace: if the liquidus isotherm is not perfectly horizontal but slightly convex, the dense liquid rejected from the mushy zone will not stay as a stable layer on the dendritic front. It will rather flow on the sides of the sample, thus enriching the region close to the crucible wall and depleting the center of the specimen. Consequently, according to the phase diagram, the liquidus temperature associated with the liquid composition will be higher in the center than closer to the wall. The curvature of the front will then have a tendency to increase. This effect is visible in the average mass composition plot on Fig. 2 (right). Whereas the nominal composition of the liquid is 22 at.%, the regions close to the wall around 1320°C have an average mass atomic fraction of more than 30 at.%.

Apart from this solute-rich liquid accumulation, the curvature of the dendritic front has a second effect on macrosegregation. It has be shown that a negative β induces liquid rejection from the mushy zone. There is no reason for the liquid expelled from the lower temperature region to go through the whole mushy zone along a 1D vertical flow. On the contrary, it may find the shortest way to exit the mushy zone, that is radially. On the left hand side of Fig. 2, the dendritic network seems less dense between 1200°C and 1270°C, showing what could be channels caused by solute-rich liquid flowing radially. In summary, the interdendritic liquid flow is not 1D, but 2D.

As gold-rich liquid exits the mushy zone, the latter becomes solute depleted and therefore shows a negative macrosegregation (Fig. 2, right). Consequently, it should be more appropriate to evaluate the microsegregation that takes place within the mushy zone by running the microsegregation model with $X_0 = 15$ at.% rather than 22 at.%. Fig. 6 traces the evolution of interfaces position with respect to temperature for such conditions during the peritectic transformation/solidification. It appears that the calculated volume fractions of (γ-Fe) and (Au) for $X_0 = 15$ at.% correspond precisely to the measurements (see Fig. 2): the volume fraction of the primary solid phase (γ-Fe) ranges from 0.8 at the peritectic temperature T_p to around 0.6 at the end of the peritectic reaction. Furthermore, the modeled temperature interval of the peritectic reaction (about 12 K) is closer to the measured value (15 K) than that modeled with the condition $X_0 = 22$ at.% (25 K).

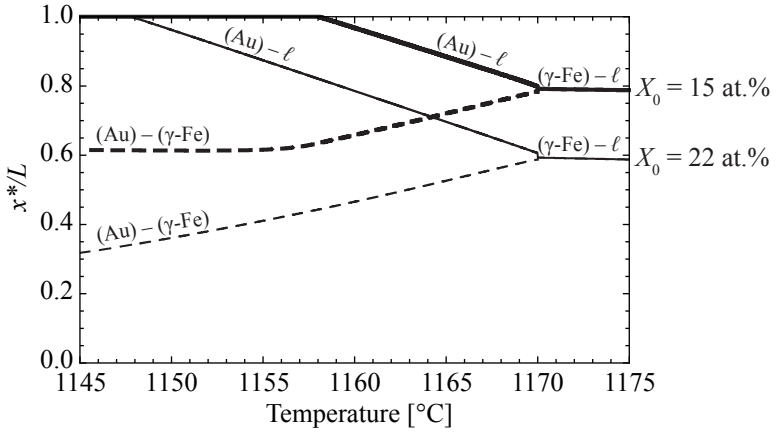

Figure 6: Calculated evolution of interface positions during peritectic reaction for an alloy of composition $X_0 = 15$ at.% (thick lines) and $X_0 = 22$ at.% (thin lines) . Plain line indicates solid–liquid interface and dashed line stands for (γ-Fe)–(Au) interface.

Finally, due to the high density of the peritectic phase (Au), the volume change of the peritectic reaction is limited (see Fig. 5). Therefore, almost no liquid flow is induced by the peritectic transformation/solidification.

Conclusions

Solidification of an Au–Fe alloy solidified at low speed in a high thermal gradient using a Bridgman furnace has been studied. Microprobe analysis as well as modeling showed that microsegregation follows the lever rule during the solidification of primary (γ-Fe), but that a composition gradient is formed in the peritectic phase (Au) during peritectic transformation/solidification.

During solidification of the primary phase, a large negative shrinkage factor β indicates that solute-rich liquid is expelled out of the mushy zone. Because of the existence of a radial thermal gradient, and due to the fact that the expelled liquid is denser that the nominal liquid, the dendritic front shape becomes more and more convex. Therefore, the liquid flows out of the mushy zone, also laterally, leading to a negative central macrosegregation. Using a lower value of c_0 in this zone, the microsegregation model predictions are in closer agreement with experiments.

Acknowledgements

The authors thank J.D. Wagnière (LSMX-EPFL) for his help with experiments and Dr. F. Bussy and J. Allibon from the *Institut de Minéralogie et Géochimie* from the University of Lausanne (UNIL, Switzerland) for microprobe measurements. Electron microscope analysis were performed at CIME (Interdisciplinary Center for Electron Microscopy at EPFL).

References

[1] H. Okamoto, *Phase diagrams of binary iron alloys*, (Materials Park, OH: ASM International, 1993).

[2] Mehrdad Vandyoussefi, "Microstructure selection during directional solidification and solid-state transformation in Fe-Ni alloys.", (Ph.D. thesis n° 3023, EPFL, Lausanne, Switzerland, 1997).

[3] D. Favez, J.D. Wagnière, and M. Rappaz, "Au–Fe alloys solidification and solid state transformation", *To be submitted to Acta Materialia*.

[4] W.S. Rasband. "ImageJ". U. S. National Institutes of Health, Bethesda, Maryland, USA, `http://rsb.info.nih.gov/ij/`, 1997-2008.

[5] E. A. Brandes and Colin James Smithells, *Smithells metals reference book*, 7th edition, (Oxford: Butterworth-Heinemann, 1999).

[6] Y. Iijima and Y. Yamazaki, "Interdiffusion between metals of widely different self-diffusion rates", *Diffusion and Defect Data. Pt A Defect and Diffusion Forum*, 237-240 (PART 1) (2005), 62–73.

[7] J. I. Akhter, E. Ahmed, and M. Ahmad, "Study of diffusion coefficients in liquid noble metals", *Materials Chemistry and Physics*, 93 (2-3) (2005), 504–507.

[8] W. Kurz and D.J. Fisher, *Fundamentals of solidification*, 4th edition, (Ütikon-Zürich, Switzerland: Trans Tech Publications, 1998).

[9] M.C. Flemings and G.E. Nereo, "Macrosegregation: Part I", *Trans. Met. Soc. AIME*, 239 (September 1967), 1149–1461.